JCB Article

Isoform-specific insulin receptor signaling involves different plasma membrane domains

Sabine Uhles, Tilo Moede, Barbara Leibiger, Per-Olof Berggren, and Ingo B. Leibiger

The Rolf Luft Center for Diabetes Research, Department of Molecular Medicine, Karolinska Institutet, S-171 76 Stockholm, Sweden

In pancreatic β-cells, insulin selectively up-regulates the transcription of its own gene and that of the glucokinase gene by signaling through the two isoforms of the insulin receptor, i.e., A-type (Ex11−) and B-type (Ex11+), using different signaling pathways. However, the molecular mechanism(s) that allows the discrete activation of signaling cascades via the two receptor isoforms remains unclear. Here we show that activation of the insulin promoter via A-type and of the glucokinase promoter via B-type insulin receptor is not dependent on receptor isoform–specific differences in internalization but on the different localization of the receptor types in the plasma membrane. Our data demonstrate that localization and function of the two receptor types depend on the 12–amino acid string encoded by exon 11, which acts as a sorting signal rather than as a physical spacer. Moreover, our data suggest that selective activation of the insulin and glucokinase promoters occurs by signaling from noncaveolae lipid rafts that are differently sensitive toward cholesterol depletion.

Introduction

Insulin exhibits a number of actions, i.e., regulation of gene transcription, translation, enzyme activities, ion flux, cell survival, etc., that are dependent on the state of development and/or differentiation of the cell type and on the cell type itself. This pleiotropic action of insulin is well appreciated, however, the underlying mechanisms are poorly understood. Selectivity in insulin signaling is currently discussed as the result of the activation of specific signal transduction pathways. This can be achieved by involving specific adaptor proteins that transduce the insulin signal in a more defined way by selectively interacting with downstream located effector proteins (Myers and White, 1996; Virkamäki et al., 1999).

The insulin receptor (IR) exists in two isoforms, as a result of alternative mRNA splicing (Seino and Bell, 1989), that either lack (type A, Ex11−) or contain (type B, Ex11+) the 12 amino acids encoded by exon 11, which are located at the COOH terminus of the α chain of the receptor. Although all cell types express both isoforms of the IR to a various degree, little is known about the mechanisms that underlie IR isoform–specific signaling. Besides the twofold higher affinity for insulin of the A-type versus the B-type IR (Mosthaf et al., 1990; McClain, 1991; Yamaguchi et al., 1991), differences in their kinase activity (Kellerer et al., 1992) as well as internalization and recycling (Vogt et al., 1991; Yamaguchi et al., 1991) have been described.

We have recently reported that in insulin-producing pancreatic β-cells, selective insulin signaling can be gained by using the two isoforms of the insulin receptor (Leibiger et al., 2001). While insulin, secreted upon glucose stimulation, activates the transcription of its own gene by signaling via IR-A/PI3K Ia/p70 s6 kinase and CaM kinase II (Leibiger et al., 1998b), it requires signaling via IR-B/PI3K C2α-like activity/PKB to activate β-cell glucokinase (βGK) gene transcription (Leibiger et al., 2001). The aim of the present study was to analyze the molecular mechanism(s) that allows the activation of different signaling cascades downstream of the two IR isoforms. Here we show that activation of the insulin promoter (via A-type IR) and of the βGK promoter (via B-type IR) is not dependent on IR isoform–specific differences in receptor internalization but is dependent on the 12 amino acids encoded by exon 11, which determine the localization of the receptor isoforms in the plasma membrane. Moreover, our data suggest that selective activation of the two promoters occurs by signaling from noncaveolae lipid rafts that are differently sensitive toward cholesterol depletion.

Address correspondence to Ingo B. Leibiger, Karolinska Institutet, Department of Molecular Medicine, The Rolf Luft Center for Diabetes Research L3, S-171 76 Stockholm, Sweden. Tel.: 46-8-5177 5725. Fax: 46-8-5177 9450. email: ingo.leibiger@molmed.ki.se

Key words: lipid rafts; fluorescent protein; signal transduction; insulin; glucokinase

Abbreviations used in this paper: βCD, β-cyclodextrin; βGK, β-cell glucokinase; FRET, fluorescence resonance energy transfer; IR, insulin receptor.

Results

Differences in IR isoform internalization are not responsible for isoform-selective up-regulation of insulin promoter and βGK promoter activities

One of the reported differences in IR isoform–specific function is their different internalization and recycling (Vogt et al., 1991; Yamaguchi et al., 1991). To test whether internalization of IR-A and IR-B is required for the activation of insulin and βGK gene transcription, respectively, we studied insulin-dependent promoter activation in β-cells that were transiently transfected with the dominant-negative mutant of dynamin-2, i.e., dynamin-2K44A. As the read-out for insulin promoter and βGK promoter activity, we used the increase in fluorescence of the reporters DsRed2 and GFP, the expression of which was driven by the respective promoters (Leibiger et al., 2001; Moede et al., 2001). Using a vector that contained the expression cassettes of both rat insulin-1 promoter–driven DsRed2 and rat βGK promoter–driven GFP not only allowed the simultaneous analysis of the two promoters in the same cell, but also improved the evaluation of additionally expressed proteins in cotransfection studies. We have recently shown that transient overexpression of the dominant-interfering dynamin-2 mutant K44A abolishes clathrin-dependent endocytosis of the Na^+-K^+ ATPase (Efendiev et al., 2002). Data by Ceresa et al. (1998) demonstrated that dominant-interfering dynamin abolishes the endocytosis of insulin receptors. As shown in Fig. 1 A, overexpression of dynamin-2K44A had no inhibitory effect on either insulin promoter–driven DsRed2 expression or βGK promoter–driven GFP expression.

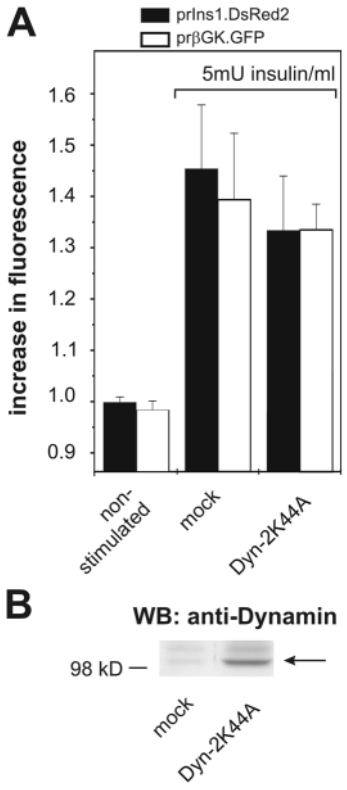

Figure 1. **Effect of dominant-interfering dynamin-2K44A on insulin-stimulated insulin promoter and βGK promoter activation.** (A) HIT T15 cells were transfected with a vector expressing both rat insulin-1 promoter–driven DsRed2 (closed bars) and rat βGK promoter–driven GFP (open bars) and with either a plasmid for the dominant-interfering dynamin-2 mutant K44A (Dyn-2K44A) or the empty vector (mock). Cells were stimulated for 5 min with 5 mU insulin/ml, and the increase of promoter activity was measured as the ratio of fluorescence obtained at 240 min versus 60 min. Data are represented as mean values ± SEM ($n \geq 12$). (B) Western blot analysis of expressed dominant-interfering dynamin-2 mutant K44A (Dyn-2K44A) versus endogenous dynamin in cells expressing the empty vector (mock). Cell lysates were separated over a 7.5–15% polyacrylamide gel, and the blot was probed with the anti-dynamin Hudy1 antibody.

Different localization and function of the IR isoforms depend on the 12 amino acids encoded by exon 11

Another possibility to explain the differences in IR isoform–specific activation of the insulin and βGK genes is the different localization of the receptors in the β-cell plasma membrane, which consequently may allow the access to different adaptor and effector proteins. To test whether IR-A and IR-B exhibit a distinct distribution in vivo, we tagged both receptor isoforms with monomeric forms of CFP (mCFP), YFP (mYFP), GFP (mGFP), or DsRed2, which exhibit a reduced aggregate formation (Zacharias et al., 2002). Using monomeric fluorescent proteins as tags excludes the possibility of artifacts in receptor distribution caused by the aggregate formation of the "wild-type" forms of the respective protein tags CFP, YFP, GFP, and DsRed. Moreover, the combination of mCFP/mYFP may allow the evaluation of hybrid formation of the IR by fluorescence resonance energy transfer (FRET) analysis (Zacharias et al., 2002). Coexpression of differently tagged receptors of the same isoform led not only to a high degree of colocalization (Fig. 2 A, a and b) but also to the generation of FRET (Fig. 2 A, d and e). On the other hand, coexpression of differently tagged IR-A and IR-B showed areas where the two IR isoforms were not colocalized (Fig. 2 A, c) and did not allow FRET (Fig. 2 A, f). To evaluate whether the observed FRET is generated by energy transfer between the two β-subunits of the same receptor (intra-receptor FRET) and whether FRET can be generated between two receptor molecules (inter-receptor FRET), we used a cell-free system for FRET analysis. Therefore, tagged IR isoforms were expressed in HIT cells, and FRET was studied in the lysates of disrupted cells (Fig. 2 B). Coexpression of IR-A–mCFP and IR-A–mYFP in the same batch of cells leads to the generation of FRET. The same was true for coexpression of IR-B–mCFP and IR-B–mYFP (not depicted). However, when we expressed mCFP-tagged and mYFP-tagged receptors of the same isoform separately in different batches of cells, disrupted the cells, and mixed the cell lysates, we observed no FRET. Neither coexpression of differently tagged IR-A and IR-B in the same batch of cells nor mixing the lysates of cells that express the two isoforms separately resulted in FRET in cell lysates. Taken together, these results led us to conclude that the two isoforms of the insulin receptor are not capable of interacting and producing FRET and that the FRET observed in cells expressing IR-A–mCFP/IR-A–mYFP or IR-B–mCFP/IR-B–mYFP

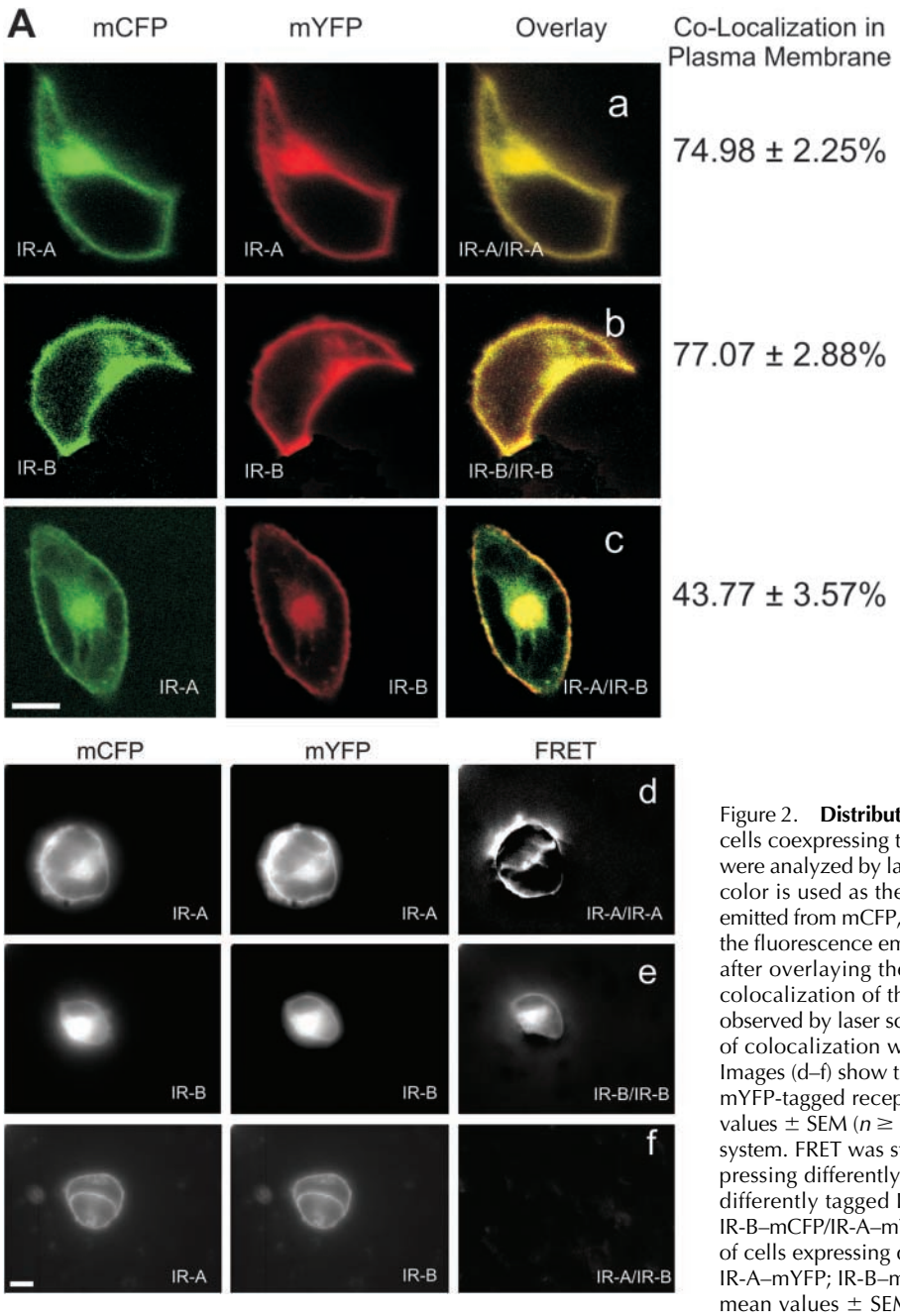

Figure 2. **Distribution of differently tagged IR isoforms.** (A) INS1 cells coexpressing tagged IR isoforms in various combinations were analyzed by laser scanning confocal microscopy. The green color is used as the digital pseudocolor for the fluorescence emitted from mCFP, and red is used as the digital pseudocolor for the fluorescence emitted from mYFP. The yellow color obtained after overlaying the mCFP and mYFP signals (a–c) indicates colocalization of the expressed IR isoforms. Distribution was observed by laser scanning confocal microscopy, and the degree of colocalization was determined by 2D scatterplot analysis. Images (d–f) show the degree of FRET obtained from mCFP- and mYFP-tagged receptor hybrids. Data are represented as mean values ± SEM ($n \geq 8$). Bars, 5 μm. (B) FRET analysis in a cell-free system. FRET was studied in lysates from batches of cells coexpressing differently tagged IR-A (IR-A–mCFP/IR-A–mYFP) or differently tagged IR-A and IR-B (IR-A–mCFP/IR-B–mYFP; IR-B–mCFP/IR-A–mYFP), and in mixed lysates of different batches of cells expressing differently tagged IR isoforms (IR-A–mCFP + IR-A–mYFP; IR-B–mCFP + IR-A–mYFP). Data are represented as mean values ± SEM ($n = 10$). (C) That tagged IR isoforms are expressed in equal amounts is shown exemplarily by Western blot analysis of expressed mGFP-tagged IR-A and IR-B versus cells expressing the empty vector (mock). Cell lysates were separated over a 4–10% polyacrylamide gel, and the blot was probed with the anti-GFP antibody JL-8.

results from intra-receptor fluorophore interaction rather than from inter-receptor interaction.

To get a quantitative assessment of the degree of colocalization within the plasma membrane, we employed the 2D scatterplot analysis (Leica). Analysis of these images showed a >70% colocalization for differently tagged IRs of the same isoform, while it showed only an ~40% colocalization when differently tagged IR-A and IR-B isoforms were coexpressed (Fig. 2 A, a–c).

To test whether the 12 amino acids encoded by exon 11 and present in the B-type receptor are responsible for the differences in localization and function of the IR isoforms, we generated a series of deletion mutants of IR-B by successive shortening the 12–amino acid string from the COOH-terminal side. Because the α chain of both isoforms ends with the identical 4–amino acid string PRPS, which directly flanks the proteolytical processing site of the pro-receptor, we decided to successively eliminate 10 amino acids in front of these 4 amino acids, thus generating deletion mutants Δ1–Δ10 (Table I). Separate overexpression of IR-B, IR-A, and all intermediates Δ1–Δ10 (Fig. 3 A) revealed that IR-B, Δ1, and Δ2 led to an enhanced activity of the βGK promoter but not of the insulin promoter in response to insulin stimulation, whereas Δ7–Δ10 and IR-A showed the opposite, i.e., pronounced insulin promoter activity but no further activation of the βGK promoter. Interestingly, expression of receptor mutants Δ3–

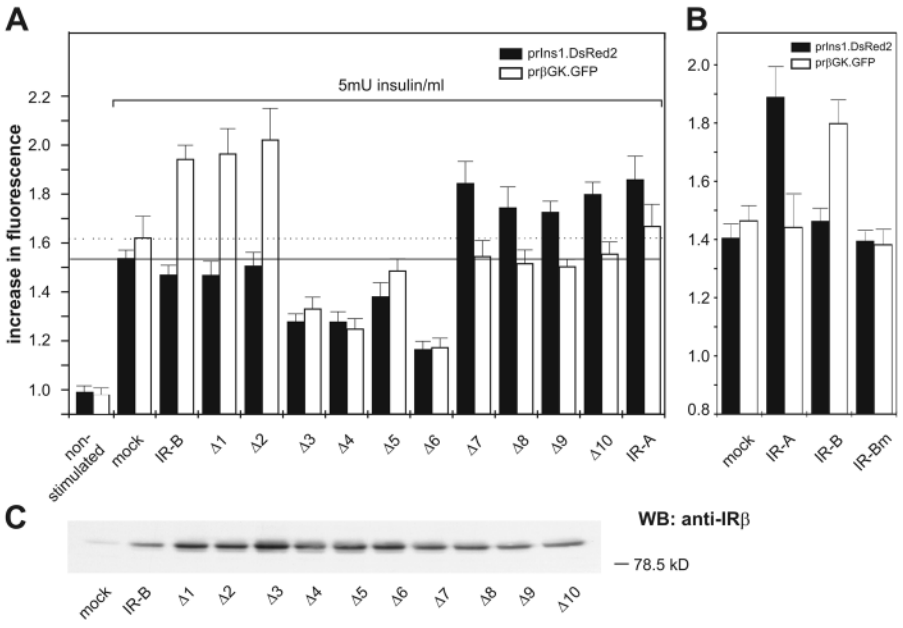

Figure 3. **Functional analysis of IR-B mutants.** Effect of overexpressed IR-B deletion mutants (A) and IR-Bm, i.e., S721V+D727V, (B) on insulin-stimulated insulin promoter and βGK promoter activation. HIT T15 cells were cotransfected with a vector containing both rat insulin-1 promoter–driven DsRed2 (closed bars) and rat βGK promoter–driven GFP (open bars), and a plasmid expressing the indicated IR variants. The increase of promoter activity was measured as a ratio of fluorescence obtained at 240 min versus 60 min after stimulation with 5 mU insulin/ml for 5 min and is represented as mean value ± SEM ($n \geq 9$). (C) Western blot analysis of expressed wild-type IR or deletion mutants versus endogenous IR in cells expressing the empty vector (mock). Cell lysates were separated over a 4–10% polyacrylamide gel, and the blot was probed with the anti-IRβ antibody insulin Rβ C-19.

Δ6 interfered with insulin-dependent up-regulation of both the insulin and βGK promoter. To test whether the simple presence of 12 amino acids, acting as a "spacer," results in the different, isoform-specific function, we mutated amino acids Ser721 and Asp727 within the 12–amino acid string of IR-B to Val, thus generating IR-Bm. As shown in Fig. 3 B, expression of IR-Bm did not allow the pronounced activation of the βGK promoter as seen with wild-type IR-B.

To test whether function of the receptor can be related to its localization, we tagged mutants Δ2, Δ3 and Δ6, Δ7 with mGFP and coexpressed them with their closest wild-type counterpart, i.e., IR-B–DsRed2 with Δ2–mGFP and Δ3–mGFP and IR-A–DsRed2 with Δ6–mGFP and Δ7–mGFP. While the biologically active mutants Δ2 and Δ7 (Fig. 3 A) colocalized with IR-B and IR-A, respectively (Fig. 4 A, a and d), the nonactive mutants Δ3 and Δ6 showed a much lower degree of colocalization with their respective wild-type receptor counterparts IR-B and IR-A (Fig. 4 A, b and c). Moreover, expression of the inactive IR-B mutant IR-Bm resulted in a low degree of colocalization with the wild-type IR-B (compare Fig. 2 A, b, with Fig. 4 A, e) and did not show an increase in colocalization with IR-A (Fig. 4 A, f). Finally, tagged receptor mutants with a below the juxtamembrane region truncated β-subunit, i.e., 23 amino acids below the transmembrane region, thus missing the last 380 amino acids of the COOH terminus, showed a colocalization of >80% with their tagged wild-type IR counterpart (Fig. 5 A, a and b), while coexpression of differently tagged IR-AΔC380 with IR-BΔC380 resulted in a low degree of colocalization (Fig. 5 A, c). These data suggest that the 12 amino acids encoded by exon 11 are responsible for both different localization and function of the two IR isoforms.

Selective IR isoform signaling involves cholesterol-sensitive membrane microdomains

An attractive hypothesis that could explain the differences in IR isoform localization and function in the selective insulin-dependent up-regulation of insulin and βGK gene expres-

Table I. **Amino acid sequences of the α chain COOH termini of wild-type IRs and deletion mutants**

Receptor type	Oligonucleotides for site-directed mutagenesis (upper strand)	Amino acid sequence (COOH terminus of α chain)
B-type		…713-VFVPRKTSSGTGAEDPRPS
Δ1	5′-CACTGGTGCCGAGCCTAGGCCATCTC-3′	…713-VFVPRKTSSGTGAEPRPS
Δ2	5′-AGGCACTGGTGCCCCTAGGCCATCTC-3′	…713-VFVPRKTSSGTGAPRPS
Δ3	5′-TTCAGGCACTGGTCCTAGGCCATCTC-3′	…713-VFVPRKTSSGTGPRPS
Δ4	5′-CTCTTCAGGCACTCCTAGGCCATCTC-3′	…713-VFVPRKTSSGTPRPS
Δ5	5′-AACCTCTTCAGGCCCTAGGCCATCTC-3′	…713-VFVPRKTSSGPRPS
Δ6	5′-GAAAAACCTCTTCACCTAGGCCATCTC-3′	…713-VFVPRKTSSPRPS
Δ7	5′-CAGAAAAACCTCTCCTAGGCCATCTC-3′	…713-VFVPRKTSPRPS
Δ8	5′-CCCAGAAAAACCCCTAGGCCATCTC-3′	…713-VFVPRKTPRPS
Δ9	5′-CGTCCCCAGAAAACCTAGGCCATCTC-3′	…713-VFVPRKPRPS
Δ10	5′-TTTTCGTCCCCAGACCTAGGCCATCTC-3′	…713-VFVPRPRPS
A-type		…713-VFVPRPS

The table shows the nomenclature of the generated IR mutants, the DNA sequence of the upper strand oligonucleotides used in the QuikChange reaction (see Materials and methods), and the resulting amino acid sequences of the COOH terminus of the IR α chain. The 12 amino acids encoded by exon 11 and present in the B-type receptor are underlined.

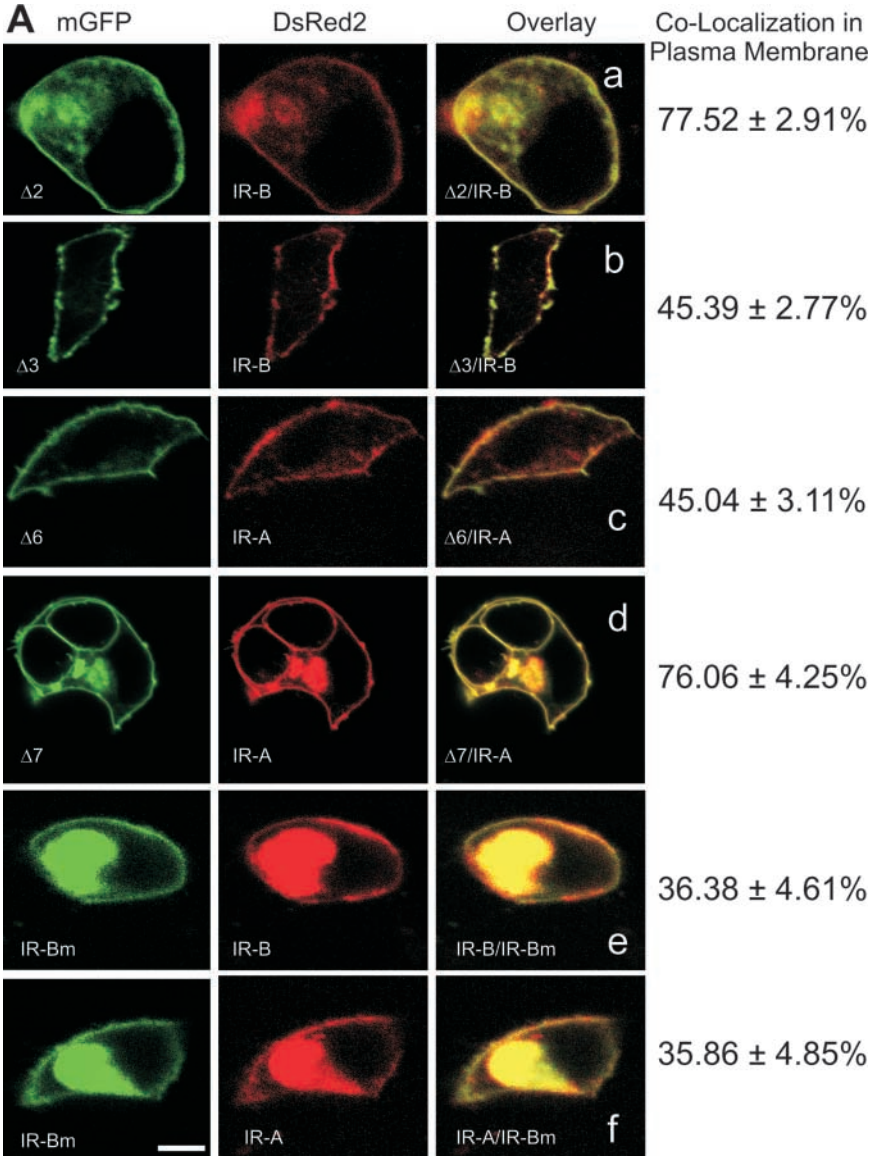

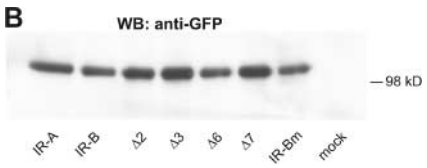

Figure 4. **Distribution of IR-B mutants.** (A) IR-B–DsRed2 and IR-A–DsRed2 were coexpressed in HIT T15 cells with mGFP-tagged deletion mutants Δ2, Δ3 and Δ6, Δ7, or mGFP-tagged IR-Bm, respectively. The green color is used as the digital pseudocolor for the fluorescence emitted from mGFP, and red is used as the digital pseudocolor for the fluorescence emitted from DsRed2. The yellow color (a–f) obtained after overlaying the mGFP and DsRed2 signals indicates colocalization of the expressed receptor variants. Distribution was observed by laser scanning confocal microscopy, and the quantitative degree of colocalization was determined by 2D scatterplot analysis. Data are presented as mean values ± SEM ($n \geq 9$). Bar, 5 μm. (B) Western blot analysis of expressed mGFP-tagged IR-A, IR-B, and mGFP-tagged mutants Δ2, Δ3, Δ6, Δ7, and IR-Bm versus cells expressing the empty vector (mock). Cell lysates were separated over a 4–10% polyacrylamide gel, and the blot was probed with the anti-GFP antibody JL-8.

sion via IR-A and IR-B, respectively, is signal transduction from different microdomains within the β-cell plasma membrane. IR-mediated signaling has been discussed in the context of lipid rafts, i.e., cholesterol-enriched membrane microdomains (for review see Bickel, 2002), however, without discriminating the IR isoform.

To test whether or not both IR isoforms are located within cholesterol-enriched plasma membrane microdomains, we coexpressed either IR-A–mYFP or IR-B–mYFP with Myr-Palm–mCFP. Myr-Palm–mCFP is a monomeric CFP variant fused with an amino acid string that allows lipid modification by myristoylation/palmitoylation and results in the localization of Myr-Palm–mCFP in cholesterol-enriched membrane domains (Zacharias et al., 2002). Expression of both combinations, i.e., IR-A–mYFP/Myr-Palm–mCFP and IR-B–mYFP/Myr-Palm–mCFP, resulted in a high degree of colocalization, which suggests that both IR-A and IR-B are mostly located within cholesterol-enriched membrane domains (Fig. 6, a and b).

Cholesterol depletion has been shown to inhibit lipid raft–dependent signaling in general (Simons and Toomre, 2000) and in IR-mediated signaling in particular (Gustavsson et al., 1996; Parpal et al., 2001; Vainio et al., 2002). To test whether cholesterol-sensitive membrane domains are involved in the insulin-dependent up-regulation of both insulin promoter and βGK promoter activity, we used β-cyclodextrin (βCD) as a tool to deplete the β-cell membrane of cholesterol. To avoid additional cholesterol depletion of intracellular membranes, we treated HIT or INS1 cells for only 10 min with 10 mM βCD and then stimulated the cells with 5 mU insulin per ml for 5 min in the presence of βCD. As shown in Fig. 7 A, treatment with 10 mM βCD abolished insulin-stimulated up-regulation of both insulin promoter and βGK promoter activities, whereas treatment of cells with α-cyclodextrin, the inactive counterpart to βCD, did not. On the other hand, treatment with βCD did not abolish PMA-induced activation of the c-fos promoter, thus excluding a generalized negative effect of the compound on stimulated gene transcription (Fig. 7 B).

Next we tested the effect of different degrees of cholesterol depletion by βCD on selective up-regulation of insulin promoter and βGK promoter activation by the two IR isoforms

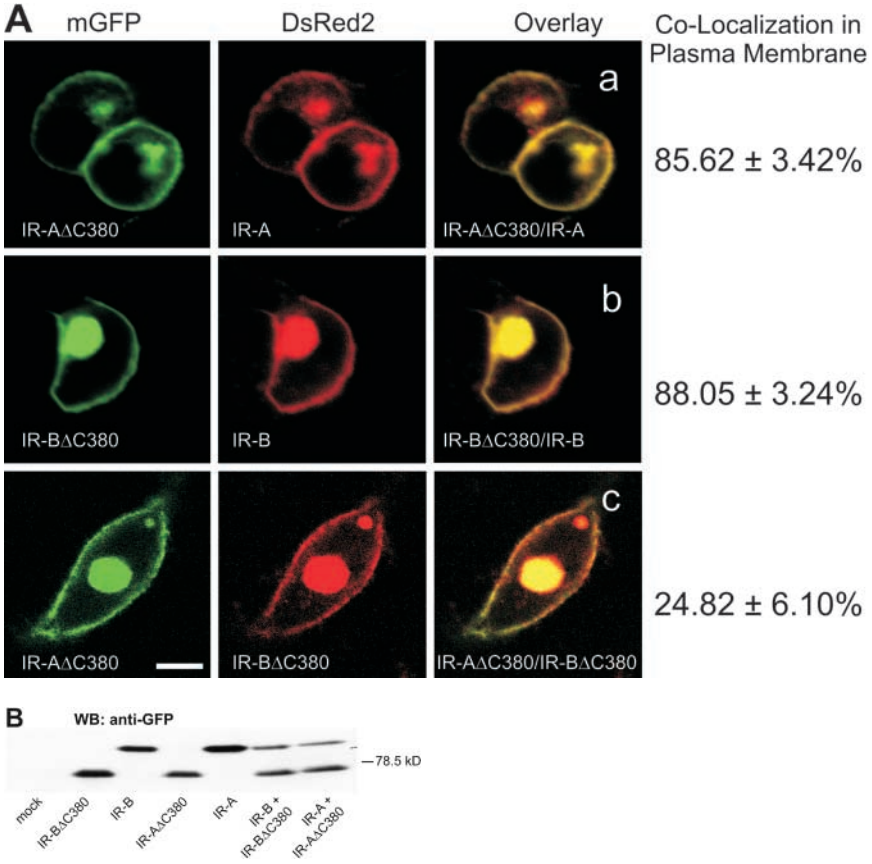

Figure 5. **Distribution of the ΔC380 mutant forms of IR-A and IR-B.** (A) HIT T15 cells were cotransfected with the combinations IR-A–DsRed2/IR-AΔC380–mGFP, IR-B–DsRed2/IR-BΔC380–mGFP, and IR-BΔC380–DsRed2/IR-AΔC380–mGFP. The green color is used as the digital pseudocolor for the fluorescence emitted from mGFP, and red is used as the digital pseudocolor for the fluorescence emitted from DsRed2. The yellow color obtained after overlaying the mGFP and DsRed2 signals (a–c) indicates colocalization of the expressed receptor variants in the plasma membrane. The distribution was observed by laser scanning confocal microscopy, and the quantitative degree of colocalization was analyzed by 2D scatterplot analysis. Data are presented as mean values ± SEM ($n \geq 9$). Bar, 5 μm. (B) Western blot analysis of expressed mGFP-tagged IR-A, IR-B, IR-AΔC380, and IR-BΔC380 versus cells expressing the empty vector (mock). Cell lysates were separated over a 4–10% polyacrylamide gel, and the blot was probed with the anti-GFP antibody JL-8.

(Fig. 7 A). While treatment of HIT cells for 10 min with 2.5 mM βCD had no effect on both insulin-stimulated insulin promoter and βGK promoter activity, treatment with 4, 5, or 6 mM βCD abolished insulin-stimulated βGK promoter but not insulin promoter activity. Finally, treatment for 10 min with 7.5 or 10 mM βCD abolished both insulin-stimulated insulin promoter and βGK promoter activity. It is noteworthy that βCD treatment did not significantly change insulin-induced activation, i.e., autophosphorylation, of either A- or B-type insulin receptor (unpublished data).

Taken together, these data show that insulin-stimulated activation of both the insulin promoter (via IR-A) and the βGK promoter (via IR-B) is sensitive to cholesterol depletion. Moreover, the data suggest that IR isoform–dependent activation of insulin and βGK gene transcription involves signaling from plasma membrane microdomains that are differently sensitive toward cholesterol depletion.

Role of caveolins in IR isoform–dependent activation of insulin and βGK promoters

Caveolae represent a subgroup of "lipid raft" microdomains that are, besides glycosphingolipids and cholesterol, enriched in caveolin-1, -2, and/or -3 (Simons and Ikonen, 1997; Brown and London, 1998; Simons and

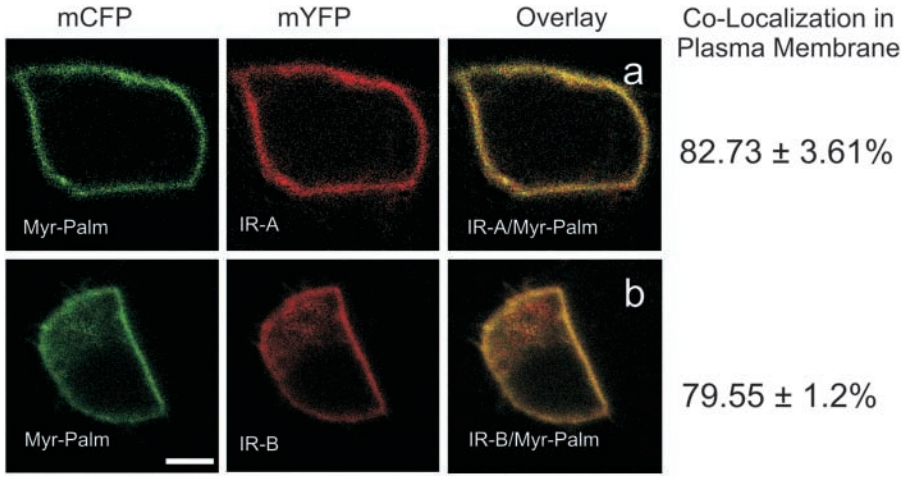

Figure 6. **Distribution of IR-A–mYFP, IR-B–mYFP, and Myr-Palm–mCFP.** INS1 cells were cotransfected with either IR-A–mYFP and Myr-Palm–mCFP or with IR-B–mYFP and Myr-Palm–mCFP. The green color is used as the digital pseudocolor for the fluorescence emitted from mCFP, and red is used as the digital pseudocolor for the fluorescence emitted from mYFP. The yellow color obtained after overlaying the mCFP and mYFP signals indicates colocalization of the expressed proteins (a and b). The colocalization observed by laser scanning confocal microscopy was quantified by 2D scatterplot analysis. Data are represented as mean values ± SEM ($n \geq 9$). Bar, 5 μm.

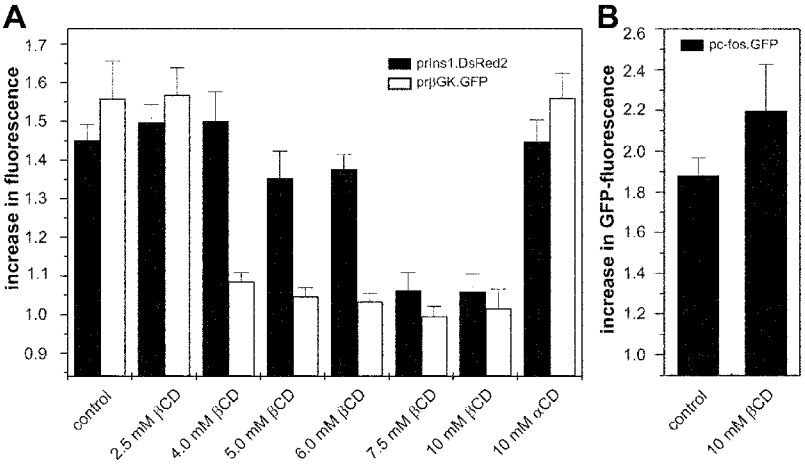

Figure 7. **Effect of cholesterol depletion on insulin-stimulated insulin promoter and βGK promoter activation.** (A) HIT T15 cells were transfected with a vector expressing both rat insulin-1 promoter–driven DsRed2 (closed bars) and rat βGK promoter–driven GFP (open bars) and treated for 10 min before and throughout stimulation with indicated amounts of βCD or αCD, respectively. (B) HIT T15 cells expressing the c-fos promoter–driven GFP were treated with 10 mM βCD and stimulated for 5 min with 100 ng PMA/ml. The increases in promoter activity were measured as ratios of fluorescence obtained at 240 min versus 60 min after stimulation and are represented as mean values ± SEM ($n \geq 9$).

Toomre, 2000) and that are thought to be involved in IR-dependent signaling (for review see Bickel, 2002). To test whether caveolins are involved in the selective signaling via the two IR isoforms in pancreatic β-cells, we first investigated the expression of caveolins in rat and mouse islets of Langerhans. RT-PCR analysis (Fig. 8 A) and cloning as well as Western blot analysis (Fig. 8 B) revealed that caveolin-1 and -2, but not caveolin-3, are expressed in mouse and rat pancreatic islets.

To understand whether caveolins are involved in IR-A–mediated activation of the insulin promoter and/or IR-B–mediated up-regulation of the βGK promoter, we employed wild-type (caveolin-1α, -1β, and -2) and dominant-interfering forms of caveolins in transient expression studies. Expression of the dominant-interfering isoforms of caveolin, i.e., Cav-3DGV and the related Cav-1DGI (Pol et al., 2001), both resulted in an almost complete loss in insulin-stimulated up-regulation of insulin promoter and βGK promoter activity (Fig. 9 A). However, coexpression of either caveolin-1α, caveolin-1β, or caveolin-2 alone as well as the combinations caveolin-1α + caveolin-2 or caveolin-1β + caveolin-2 had no effect upon insulin-stimulated insulin promoter or βGK promoter activity (Fig. 9 A). These data suggest that, although present in insulin-producing cells, caveolin-1α, -1β, and -2 do not seem to be involved in either IR-A–dependent up-regulation of the insulin gene or in IR-B–dependent βGK promoter activation. This does not necessarily exclude that the respective IRs reside in caveolin-containing lipid domains, but makes a direct and/or indirect action of caveolins themselves unlikely. The observed abolishing effect of dominant-negative caveolins, i.e., Cav-3DGV and Cav-1DGI, on insulin-stimulated insulin promoter and βGK promoter activation may be explained by the fact that these mutants sequester cholesterol intracellularly, which leads to a decrease in cell surface cholesterol and thus interferes with the formation of lipid microdomains (Luetterforst et al., 1999; Pol et al., 2001). However, caveolae only represent a subset of lipid rafts. The involvement of noncaveolin-containing lipid rafts in IR-mediated signaling was shown in human HuH7 hepatoma cells that express IRs but lack caveolae (Vainio et al., 2002).

Discussion

In the present study, we sought to analyze the molecular mechanisms that underlie the selective activation of different signaling cascades downstream of the two isoforms of the IR, e.g., IR-A and IR-B. Expression of the dominant-interfering form of dynamin-2, dynamin-2K44A, showed

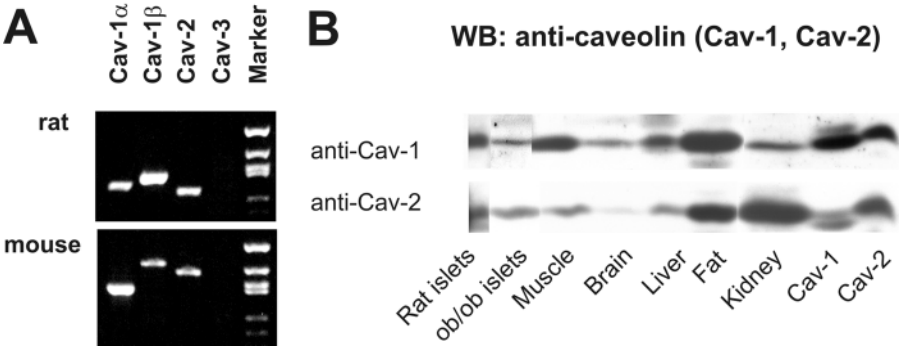

Figure 8. **Expression of caveolins in rat and mouse pancreatic islets.** (A) RT-PCR was performed on mRNA prepared from rat and mouse pancreatic islets using primer combinations and PCR conditions as described in the Materials and methods. RT-PCR products for caveolin-1α, -1β, -2, and -3 were analyzed by agarose gel electrophoresis. DNA fragments obtained from HpaII-digested pBluescriptKSII(+) plasmid (Stratagene) served as length markers (length in bp: 710, 489, 404, 364, 242, and 190). RT-PCR products for rat caveolin-1α, -1β, and -2 resulted in DNA fragments showing the following lengths (in bp): 308 (Cav-1α), 354 (Cav-1β), and 283 (Cav-2), respectively. RT-PCR products for mouse caveolins resulted in DNA fragments of 379 (Cav-1α), 533 (Cav-1β), and 469 bp (Cav-2), respectively. No RT-PCR product was obtained for either rat or mouse caveolin-3. (B) Western blot analysis of membrane fractions obtained from rat and mouse islets and different rat tissues using antibodies against mouse caveolin-1 and mouse caveolin-2.

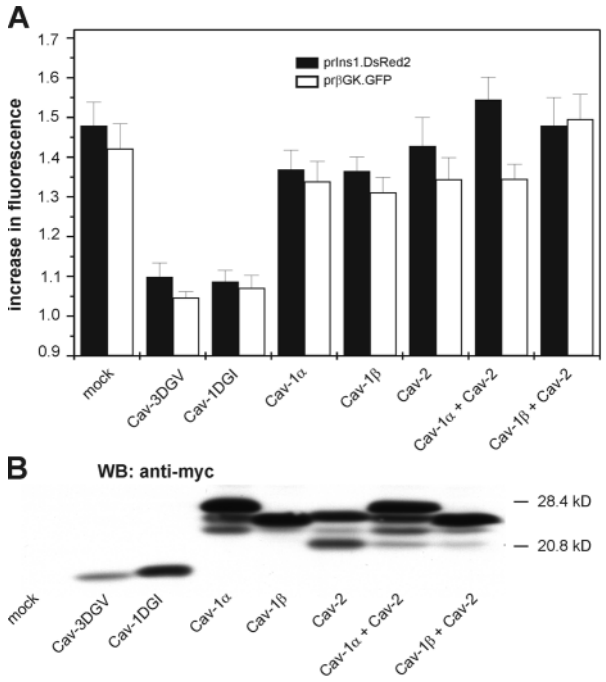

Figure 9. **Effect of overexpressed wild-type and dominant-interfering forms of caveolin on insulin-stimulated insulin promoter and βGK promoter activation.** (A) HIT T15 cells were cotransfected with a vector expressing both rat insulin-1 promoter–driven DsRed2 (closed bars) and rat βGK promoter–driven GFP (open bars) and with one of the indicated wild-type or dominant-interfering forms of caveolin. The increases in promoter activity were measured as ratios of fluorescence obtained at 240 min versus 60 min after stimulation with 5 mU insulin/ml and are represented as mean values ± SEM ($n \geq 9$). (B) Western blot analysis of expressed myc/His-tagged caveolins-1α, -1β, and -2 and of myc/His-tagged dominant-interfering forms Cav-3DGV and Cav-1DGI versus cells expressing the empty vector (mock). Cell lysates were separated over a 10–20% polyacrylamide gel, and the blot was probed with the anti-myc antibody anti-myc tag clone 9E10.

that the activation of the insulin promoter via IR-A and that of the βGK promoter via IR-B is not dependent on IR isoform–specific differences in receptor internalization and that the signals responsible for insulin-dependent up-regulation of the two genes originate from membrane-standing IRs rather than from internalized receptor complexes. This is in agreement with a study showing that expression of dominant-interfering dynamin does not interfere with immediate insulin effects in 3T3L1 adipocytes and H4IIE hepatoma cells, such as glucose uptake, glycogen synthesis, and lipogenesis, thus demonstrating that most acute actions of insulin are largely independent of IR endocytosis (Ceresa et al., 1998).

The present data clearly suggest a relationship between the location and function of the IR in the IR isoform–dependent activation of the insulin promoter and βGK promoter activities in the pancreatic β-cell. Our data show that location and function of the IR are determined by the 12 amino acids encoded by exon 11 of the IR gene. (a) While differently tagged receptors of the same isoform show a high degree of colocalization (>70%), coexpression of tagged IR-A and IR-B shows a much lower degree of colocalization (~40%). (b) Deletion mutants that still allow colocalization with their wild-type receptor counterpart (i.e., Δ1 and Δ2 with IR-B and Δ7–Δ10 with IR-A) also allow the pronounced activation of the βGK and insulin promoters, while mutants with a low degree of colocalization (Δ3–Δ6) are biologically inactive. The observation that mutation of two amino acids within the 12–amino acid string encoded by exon 11 results in both loss of function and shift in localization in the plasma membrane not only supports the view that the function of the IR is linked to localization, but also suggests that these 12 amino acids do not simply function as a physical "spacer" but may represent a specific protein motif. This together with the data obtained with the COOH-terminally truncated IR isoforms IR-AΔC380 and IR-BΔC380 imply that the 12 amino acids encoded by exon 11 represent a signal involved in the IR isoform–specific sorting of the receptor to different plasma membrane microdomains.

Both IR-A and IR-B are localized in cholesterol-containing plasma membrane domains, and their function in insulin-dependent up-regulation of the insulin and βGK promoters is sensitive toward cholesterol depletion in general. However, our data show that IR isoform–dependent activation of the two promoters has a different degree of sensitivity to cholesterol depletion.

Caveolae represent a subgroup of lipid raft microdomains that are, besides glycosphingolipids and cholesterol, enriched in caveolin-1, -2, and/or -3 (Simons and Ikonen, 1997; Brown and London, 1998; Simons and Toomre, 2000). An increasing body of evidence suggests direct and/or indirect involvement of caveolins in IR-dependent signaling (for review see Bickel, 2002). The role of caveolins in this process was mainly studied in adipocytes/preadipocytes and led, at first glance, to contradictory results (Bickel, 2002). Reports show that IRs reside in caveolae (Gustavsson et al., 1999), that the IR has a consensus binding site for the interaction with caveolin (Couet et al., 1997), that interaction of IRs with caveolins leads to an increase in IR tyrosine kinase activity (Yamamoto et al., 1998; Nystrom et al., 1999), and that caveolin-1 is a substrate for the tyrosine kinase of the IR (Kimura et al., 2002). Other studies suggest that IRs do not reside in caveolin-enriched plasma membrane domains (Müller et al., 2001; Souto et al., 2003) and that caveolins are not an absolute requirement for insulin signaling (Vainio et al., 2002). Our data suggest that, although expressed in pancreatic β-cells, caveolins are not involved in the IR isoform–dependent activation of the insulin and the βGK gene.

Taken together, our data imply that IR isoform–dependent activation of the insulin and βGK promoters results from IR-mediated signaling from different plasma membrane microdomains. This may mechanistically explain the access to different adaptor proteins and the subsequent activation of selective signaling pathways, as previously shown by us (Leibiger et al., 2001).

Materials and methods

RT-PCR cloning of caveolins

Expression of caveolins at the mRNA level in pancreatic islets prepared from Wistar rats and ob/ob mice was analyzed by RT-PCR using primer pairs for mouse caveolin-1α (5′-ATGGCAGACGAGGTGACTGA-3′ and 5′-GATCG-

CAGAAGGTATGGACG-3′), rat caveolin-1α (5′-AATACGTAGACTCCG-AGG-3′ and 5′-GAAGATGGTAGACAGCAAGC-3′), mouse caveolin-1β (5′-AGCCAGGCTGACTCTTGACT-3′ and 5′-CGCAGAAGGTATGGACG-TAG-3′), rat caveolin-1β (5′-GCAGACGAGGTGAATGAGAA-3′ and 5′-GATGGAATAGACACGGCTGA-3′), mouse caveolin-2 (5′-CGATGTGCAG-CTCTTCATGG-3′ and 5′-TGGTCAGTCGTGGCTCAGTT-3′), rat caveolin-2 (5′-ATCCTCACCAGCTCAACTCT-3′ and 5′-CTCTTCCATATCGTCTGCAC-3′), mouse caveolin-3 (5′-TCAACGATACCAGCCACAAG-3′ and 5′-AAGG-TGCGGATACACAGTGA-3′), and rat caveolin-3 (5′-ATGATGACCGAAGA-GCACAC-3′ and 5′-GCAGAAGGAGATACAGGCAA-3′).

To obtain full-length cDNAs containing the open reading frames for mouse caveolins, the following primer combinations were used: caveolin-1α (5′-AACCTCCTCAGAGCCTG-3′ and 5′-CTGCGAGAGCAACTTGG-3′), caveolin-1β (5′-GCCAGGCTGACTCTTGA-3′ and 5′-CTGCGAGAGC-AACTTGG-3′), and caveolin-2 (5′-AGCCACTCTTGCAACGCCAG-3′ and 5′-TGAGTGGTCAGTCGTGGCTC-3′).

RNA was isolated from 50 islets using the RNeasy kit (QIAGEN). The RNA was reverse transcribed using the RT-PCR kit from Stratagene. Aliquots of the obtained cDNA were used for PCR. PCR products were run on a 2% agarose gel, and the DNA was eluted and cloned into pCRII using the TA cloning kit (Invitrogen). All subcloned DNA fragments were analyzed by DNA sequencing.

Expression constructs

IR constructs. The construction of pRcCMVi.hIR(A) and pRcCMVi.hIR(B) and their GFP- and DsRed-tagged variants was described previously (Leibiger et al., 2001). The DsRed2-tagged IR isoforms were generated by exchanging the GFP-cDNA in pRcCMVi.hIR(A)–GFP and pRcC-MVi.hIR(B)–GFP versus the cDNA for DsRed2, obtained from pDsRed2-N1 (CLONTECH Laboratories, Inc.). To obtain IR isoforms tagged with monomeric GFP (mGFP), amino acids Ala^{206} to Lys^{206} of the GFP protein in pRcCMVi.hIR(A)–GFP and pRcCMVi.hIR(B)–GFP were changed by site-directed mutagenesis. To generate pRcCMVi.hIR(A)–mYFP and pRcC-MVi.hIR(B)–mYFP, we exchanged the GFP cassette in pRcCMVi.hIR(A)–GFP and pRcCMVi.hIR(B)–GFP with the cDNA encoding the monomeric YFP version "Venus" (Nagai et al., 2002) by XbaI/ClaI digestion. The parent plasmid containing the cDNA for Venus was provided by A. Miyawaki (Brain Science Institute, RIKEN, Saitama, Japan). The monomeric Venus form (mYFP) was created by changing Ala^{206} to Lys^{206}. To obtain IR forms tagged with monomeric CFP (mCFP), we first introduced a ClaI site by site-directed mutagenesis into pcDNA3.Myr–mCFP, which allowed subcloning of the mCFP cassette in-frame via ClaI/XbaI digestion into the ClaI/XbaI-opened pRcCMVi.hIR(A)–mYFP and pRcCMVi.hIR(B)–mYFP, thus creating pRcCMVi.hIR(A)–mCFP and pRcCMVi.hIR(B)–mCFP.

Deletion mutants of the human IR-B receptor were generated by site-directed mutagenesis on pRcCMVi.hIR(B) and pRcCMVi.hIR(B)–mGFP using the oligonucleotides listed in Table I, thus generating tagged and non-tagged deletion variants Δ1-Δ10.

Plasmids pRcCMVi.hIR(A)ΔC380–mGFP and pRcCMVi.hIR(B)ΔC380–mGFP were generated by first changing AGT, coding for Ser 24 amino acids downstream the transmembrane region, to ATC, thereby creating a ClaI site. The final expression constructs were obtained by ClaI digestion and religation of the plasmid. Plasmids encoding tagged and untagged IR-B mutant IR-Bm, i.e., $Ser^{721}Val + Asp^{727}Val$, were generated by QuikChange mutagenesis exchanging the respective codons by GTC.

Caveolin constructs. Plasmids pcDNA3.myc/His.Cav-3 and pcDNA3.myc/His.Cav-3DGV were provided by J.E. Pessin (University of Iowa, Iowa City, IA). To obtain expression constructs for mouse caveolin-1α, -1β, -2, and -1DGI, we first introduced an Asp718 site upstream of the ATG, a Kozak sequence, and an ApaI site by changing the stop codon TGA to GGG in the cDNAs of the respective caveolin isoforms (Cav-1α, Cav-1β, and Cav-2). The final expression constructs were generated by exchanging the caveolin-3 cDNA in pcDNA3.myc/His.Cav-3 versus the respective cDNAs for Cav-1α, Cav-1β, and Cav-2 by ApaI/Asp718 digestion. To generate Cav-1DGI, we changed AGT TTC (Ser^{49} Phe^{50}) to ACC ATG, thus providing a translation start and Kozak sequence, and introduced an Asp718 site in front of the Kozak sequence. ApaI/Asp718 digestion allowed us to introduce the Cav-1DGI cassettes into the ApaI/Asp718-opened pcDNA3.myc/His backbone.

Other. The vector containing the two expression cassettes, i.e., for rat insulin-1 promoter–driven DsRed2 and for rat βGK promoter–driven GFP, was generated as follows. First, we exchanged the SV40 promoter-EGFP cassette in pd2EGFP-promoter (CLONTECH Laboratories, Inc.) versus the rat βGK promoter–GFP cassette from pB.rβGK.GFP (Leibiger et al., 2001), generating pd.rβGK.GFP.SV40pA. Next, we introduced a SmaI and a XhoI site into pd.rβGK.GFP.SV40pA by site-directed mutagenesis and introduced, using these sites, the expression cassette for rIns1.DsRed2-bGHpA from pB.rIns1.DsRed2, generating pd.rIns1.DsRed2.bGHpA/rβGK.GFP.SV40pA.

All mutations were performed by using the QuikChange Mutagenesis kit (Stratagene), and respective oligonucleotides were purchased from Proligo. All constructions were verified by DNA sequence analysis.

Plasmid pc-fos.GFP was generated as previously described (Leibiger et al., 1998a). The expression construct for Myr-Palm–mCFP was provided by R.Y. Tsien (University of California, San Diego, La Jolla, CA) and was previously described (Zacharias et al., 2002). Construction of the expression vector for the dominant-negative mutant dynamin-2K44A was previously described (Efendiev et al., 2002).

Cell culture and transfection

HIT-T15 cells were obtained from American Type Culture Collection and cultured in RPMI 1640 culture medium supplemented with 100 U/ml penicillin, 100 μg/ml streptomycin, 2 mM glutamine, and 10% fetal calf serum at 5% CO_2 and 37°C. INS1 cells were obtained from C.B. Wollheim (Centre Médical Universitaire, Geneva, Switzerland) and cultured in RPMI 1640 culture medium supplemented with 100 U/ml penicillin, 100 μg/ml streptomycin, 2 mM glutamine, 10% fetal calf serum, 1 mM pyruvate, 10 mM Hepes, and 50 μM β-mercaptoethanol at 5% CO_2 and 37°C.

For transient expression studies, cells were grown on 24-mm glass coverslips and transfected overnight using the lipofectamine technique. After transfection, cells were cultured for a further 24 h in fully supplemented RPMI 1640 culture medium. When performing promoter studies, transfected cells were incubated overnight in fully supplemented RPMI 1640 culture medium at 0.1 mM glucose and stimulated for 5 min with 5 mU insulin/ml, or for 15 min with 100 ng PMA/ml in fully supplemented RPMI 1640 culture medium when studying c-fos promoter–driven GFP expression. The cyclodextrin studies were performed in RPMI 1640 culture medium at 0.1 mM glucose containing 0.5% BSA instead of 10% FCS.

Expression of insulin receptor variants, dominant-negative dynamin-2, and wild-type and dominant-negative caveolins was verified by Western blot analysis (see Western blot analysis section).

Online monitoring of GFP and DsRed2 expression

Expression of DsRed2 and GFP was detected using digital imaging fluorescence microscopy as previously described (Leibiger et al., 1998a,b, 2001; Moede et al., 2001). In brief, glass coverslips with transfected cells were placed in a perifusion chamber and mounted on an inverted microscope (Zeiss Axiovert 133TV; Carl Zeiss MicroImaging, Inc.) equipped with a Zeiss plan NEOFLUAR x25/0.8 Imm Korr lens (Carl Zeiss MicroImaging, Inc.). During the experiment, the cells were kept at 37°C and perifused with fully supplemented RPMI 1640 culture medium at 0.1 mM glucose or with RPMI 1640 culture medium at 0.1 mM glucose containing 0.5% BSA instead of 10% FCS (cyclodextrin experiments). Excitation light was obtained from a SPEX fluorolog-2 MM1T11I spectrofluorometer (Spex Industries). The following settings were used: for GFP detection, excitation at 485 nm, a 505-nm dicroic mirror, and a 505–535-nm band-pass emission filter; for DsRed2 excitation at 558 nm, a 565-nm dicroic mirror and a 580–620-nm band pass emission filter. Fluorescence was imaged using a cooled CCD camera (CH250 with KAF 1400; Photometrics) connected to an imaging system (Inovision). Online monitoring was initiated 60 min after start of stimulation, and cells to be monitored were chosen randomly in 6–12 fields of view containing at least 9 cells. For calculation, the fluorescence intensity of an individual cell at the beginning of the experiment (t = 60 min after start of stimulation) was set as 1. The fluorescence intensity of each monitored cell was followed over time and calculated relative to its intensity at t = 60 min. Fluorescence intensities were calculated by using the Isee software for UNIX (Inovision).

Confocal microscopy and colocalization analysis

Laser scanning confocal microscopy was performed using a Leica TCS SP2 confocal microscope equipped with a Leica HCX Pl Apo x63/1.20/0.17 UV objective lens as previously described (Leibiger et al., 2001). The following settings were used: for mGFP and DsRed2 fluorescence, excitation wavelength 488 nm (Ar laser) and 543 nm (HeNe laser), a 488/543 double dicroic mirror, and detection at 505–525 nm for mGFP and 605–670 nm for DsRed2; for mCFP and mYFP detection, excitation wavelength 458 nm for mCFP and 514 nm for mYFP (Ar laser), a 458/514 double dicroic mirror, and detection at 465–495 nm (mCFP) and 535–600 nm (mYFP). To eliminate fluorophore cross contamination, detection of mCFP and mYFP was performed using the "between lines" sequential scan mode of the confocal software.

Colocalization of mGFP/DsRed2 and mCFP/mYFP fluorescence within the plasma membrane was quantified using the 2D scatterplot analysis

function of the Leica confocal software version 2.5. To exclude signals originating from the cytoplasm or noncellular sources, the analysis was limited to the plasma membrane by using the "region of interest" feature of the Leica confocal software.

FRET analysis

FRET analysis was performed by digital imaging fluorescence microscopy as described in the section Online monitoring of GFP and DsRed2 expression. The following filter settings were used: for detection of mCFP fluorescence, excitation 435 nm, a 455-nm dicroic mirror, and a 460–500-nm band pass filter; for mYFP detection, excitation 495 nm, a 505-nm dicroic mirror, and a 520–550-nm band pass filter; for detection of the FRET signal, excitation 435 nm, a 455-nm dicroic mirror, and a 520–550-nm band pass filter. The FRET image was generated by linear unmixing as previously described (Zimmermann et al., 2002) using the FRET, mCFP, and mYFP signals as raw data.

For the analysis of FRET in cell lysates, cells were transfected with plasmids expressing IR-A–mCFP + IR-A–mYFP, IR-B–mCFP + IR-B–mYFP, IR-A–mCFP + IR-B–mYFP, IR-B–mCFP + IR-A–mYFP, IR-A–mCFP, IR-A–mYFP, IR-B–mYFP, and IR-B–mCFP. The cells were washed and lysed as described for Western blot analysis (cell lysates).

The fluorescence emission from the lysates was analyzed by digital imaging fluorescence microscopy as described in the section Online monitoring of GFP and DsRed2 expression. The ratio of the FRET signal to the CFP signal was used as a measure of FRET to correct for variations in fluorescence intensities caused by differences in transfection efficiency and expression levels.

Western blot analysis

Lysates for membrane preparation were obtained from Wistar rat and ob/ob mice islets and rat muscle, brain, liver, fat, and kidney. Islets and tissues were washed three times with HB buffer (12 mM Hepes, 300 mM mannitol, pH 7.6, 1 mM PMSF, 0.5 μg/ml pepstatin, 0.5 μg/ml aprotinin, and 0.5 μg/ml antipain), centrifuged for 1 min at 20,000 *g*, resuspended in HB buffer, and homogenized for 1 min using a glass–glass homogenizer followed by passing the homogenate five times through an insulin syringe needle (0.33 × 13 mm/29 G × 1/2). The homogenate was centrifuged for 5 min at 600 *g*. The pellet was homogenized again and centrifuged for 5 min at 600 *g*, and the supernatant was combined with the one collected before. The supernatants were centrifuged for 20 min at 20,000 *g*, and the new supernatants were collected and centrifuged at 60,000 *g* for 30 min. The pellets were resuspended in 200 μl HB buffer. After adding 200 μl of percoll (Sigma-Aldrich) and 800 μl HB buffer, the samples were again homogenized and centrifuged for 30 min at 70,000 *g*. The fraction between the aqueous and the percoll phase was collected, and the amount of protein was measured by the Bradford method. All working steps were performed either at 4°C or on ice.

Western blot analysis was performed by separating the membrane fractions on a 7.5–15% SDS-polyacrylamide gel (buffering system according to Laemmli) and electrotransfer to PVDF membrane. The membrane was blocked with 5% nonfat dried milk in TBS (pH 7.6) for 1 h, incubated overnight at 4°C with the respective antibodies in TBS containing 5% nonfat dried milk, and washed with TBS containing 0.1% Tween20. Immunoreactivity was detected with horseradish peroxidase–conjugated secondary antibodies using the ECL system (Amersham Biosciences). The following antibodies were employed: mouse caveolin-1, mouse caveolin-2, and mouse caveolin-3 (all from Transduction Laboratories).

Expression of insulin receptor variants, dominant-negative dynamin-2, and wild-type and dominant-negative caveolins was verified in cell lysates by Western blot analysis. Here, after washing with PBS, cells were lysed in 137 mM NaCl, 2.7 mM KCl, 1 mM $MgCl_2$, 4 mM Na_3VO_4, 1% Triton X-100, 10% glycerol, 20 mM Tris, pH 8.0, 1 μg/ml aprotinin, 1 mM PMSF, and 10 mM NaF. Western blot analysis was performed as described in the previous paragraphs. Expression of nontagged insulin receptor variants using insulin Rβ (C-19) antibody (Santa Cruz Biotechnology, Inc.) showed a more than twofold overexpression when compared with the endogenous receptor levels. Expression levels of tagged insulin receptor variants (mGFP) and tagged caveolins (myc) were verified by Western blot analysis using anti-GFP antibody JL-8 (CLONTECH Laboratories, Inc.) and anti-myc tag clone 9E10 antibody (Upstate Biotechnology), respectively. Expression of dominant-negative dynamin-2, Dyn2-K44A, analyzed by Western blotting using the anti-dynamin Hudy1 antibody (Upstate Biotechnology), showed a 2.5-fold expression over endogenous dynamin levels.

This work was supported by funds from Karolinska Institutet and grants from the Swedish Research Council (31X-12549, 31X-13394, and 31X-14303), the Swedish Diabetes Association, the National Institutes of Health (DK58508), Juvenile Diabetes Research Foundation, Berth von Kantzows Foundation, and Novo Nordisk Foundation.

Submitted: 18 June 2003
Accepted: 3 November 2003

References

Bickel, P.E. 2002. Lipid rafts and insulin signaling. *Am. J. Physiol. Endocrinol. Metab.* 282:E1–E10.

Brown, D.A., and E. London. 1998. Functions of lipid rafts in biological membranes. *Annu. Rev. Cell Dev. Biol.* 14:111–136.

Ceresa, B.P., A.W. Kao, S.R. Santeler, and J.E. Pessin. 1998. Inhibition of clathrin-mediated endocytosis selectively attenuates specific insulin receptor signal transduction pathways. *Mol. Cell. Biol.* 18:3862–3870.

Couet, J., S. Li, T. Okamoto, T. Ikezu, and M.P. Lisanti. 1997. Identification of peptide and protein ligands for the caveolin-scaffolding domain. Implications for the interaction of caveolin with caveolae-associated proteins. *J. Biol. Chem.* 272:6525–6533.

Efendiev, R., G.A. Yudowski, J. Zwiller, B. Leibiger, A.I. Katz, P.O. Berggren, C.H. Pedemonte, I.B. Leibiger, and A.M. Bertorello. 2002. Relevance of dopamine signals anchoring dynamin-2 to the plasma membrane during Na^+,K^+-ATPase endocytosis. *J. Biol. Chem.* 277:44108–44114.

Gustavsson, J., S. Parpal, and P. Strålfors. 1996. Insulin-stimulated glucose uptake involves the transition of glucose transporters to a caveolae-rich fraction within the plasma membrane: implications for type II diabetes. *Mol. Med.* 2:367–372.

Gustavsson, J., S. Parpal, M. Karlsson, C. Ramsing, H. Thorn, M. Borg, M. Lindroth, K.H. Peterson, K.E. Magnusson, and P. Strålfors. 1999. Localization of the insulin receptor in caveolae of adipocyte plasma membrane. *FASEB J.* 13:1961–1971.

Kellerer, M., R. Lammers, B. Ermel, S. Tippmer, B. Vogt, B. Obermaier-Kusser, A. Ullrich, and H.U. Häring. 1992. Distinct α-subunit structures of human insulin receptor A and B variants determine differences in tyrosine kinase activities. *Biochemistry.* 31:4588–4596.

Kimura, A., S. Mora, S. Shigematsu, J.E. Pessin, and A.R. Saltiel. 2002. The insulin receptor catalyzes the tyrosine phosphorylation of caveolin-1. *J. Biol. Chem.* 277:30153–30158.

Leibiger, B., T. Moede, T. Schwarz, G.R. Brown, M. Köhler, I.B. Leibiger, and P.O. Berggren. 1998a. Short-term regulation of insulin gene transcription by glucose. *Proc. Natl. Acad. Sci. USA.* 95:9307–9312.

Leibiger, B., I.B. Leibiger, T. Moede, S. Kemper, R.N. Kulkarni, C.R. Kahn, L.M. de Vargas, and P.O. Berggren. 2001. Selective insulin signaling through A and B insulin receptors regulates transcription of insulin and glucokinase genes in pancreatic β cells. *Mol. Cell.* 7:559–570.

Leibiger, I.B., B. Leibiger, T. Moede, and P.O. Berggren. 1998b. Exocytosis of insulin promotes insulin gene transcription via the insulin receptor/PI-3 kinase/p70 s6 kinase and CaM kinase pathways. *Mol. Cell.* 1:933–938.

Luetterforst, R., E. Stang, N. Zorzi, A. Carozzi, M. Way, and R.G. Parton. 1999. Molecular characterization of caveolin association with the Golgi complex: identification of a cis-Golgi targeting domain in the caveolin molecule. *J. Cell Biol.* 145:1443–1459.

McClain, D.A. 1991. Different ligand affinities of the two insulin receptor splice variants are reflected in parallel changes in sensitivity for insulin action. *Mol. Endocrinol.* 5:734–739.

Moede, T., B. Leibiger, P.O. Berggren, and I.B. Leibiger. 2001. Online monitoring of stimulus-induced gene expression in pancreatic β-cells. *Diabetes.* 50(Suppl. 1):S15–S19.

Mosthaf, L., K. Grako, T.J. Dull, L. Coussens, A. Ullrich, and D.A. McClain. 1990. Functionally distinct insulin receptors generated by tissue-specific alternative splicing. *EMBO J.* 9:2409–2413.

Müller, G., C. Jung, S. Wied, S. Welte, H. Jordan, and W. Frick. 2001. Redistribution of glycolipid raft domain components induces insulin-mimetic signaling in rat adipocytes. *Mol. Cell. Biol.* 21:4553–4567.

Myers, M.G., Jr., and M.F. White. 1996. Insulin signal transduction and the IRS proteins. *Annu. Rev. Pharmacol. Toxicol.* 36:615–658.

Nagai, T., K. Ibata, E.S. Park, M. Kubota, K. Mikoshiba, and A. Miyawaki. 2002. A variant of yellow fluorescent protein with fast and efficient maturation for cell-biological applications. *Nat. Biotechnol.* 20:87–90.

Nystrom, F.H., H. Chen, L.N. Cong, Y. Li, and M.J. Quon. 1999. Caveolin-1 interacts with the insulin receptor and can differently modulate insulin sig-

naling in transfected Cos-7 cells and rat adipocytes. *Mol. Endocrinol.* 13: 2013–2024.

Parpal, S., M. Karlsson, H. Thorn, and P. Strålfors. 2001. Cholesterol depletion disrupts caveolae and insulin receptor signaling for metabolic control via insulin receptor substrate-1, but not for mitogen-activated protein kinase control. *J. Biol. Chem.* 276:9670–9678.

Pol, A., R. Luetterforst, M. Lindsay, S. Heino, E. Ikonen, and R.G. Parton. 2001. A caveolin dominant negative mutant associates with lipid bodies and induces intracellular cholesterol imbalance. *J. Cell Biol.* 152:1057–1070.

Seino, S., and G.I. Bell. 1989. Alternative splicing of human insulin receptor messenger RNA. *Biochem. Biophys. Res. Commun.* 159:312–316.

Simons, K., and E. Ikonen. 1997. Functional rafts in cell membranes. *Nature.* 387: 569–572.

Simons, K., and D. Toomre. 2000. Lipid rafts and signal transduction. *Nat. Rev. Mol. Cell Biol.* 1:31–39.

Souto, R.P., G. Vallega, J. Wharton, J. Vinten, J. Tranum-Jensen, and P.F. Pilch. 2003. Immunopurification and characterization of rat adipocyte caveolae suggest their dissociation from insulin signaling. *J. Biol. Chem.* 278:18321–18329.

Vainio, S., S. Heino, J.-E. Månsson, P. Fredman, E. Kuismanen, O. Vaarala, and E. Ikonen. 2002. Dynamic association of human insulin receptor with lipid rafts in cells lacking caveolae. *EMBO Rep.* 3:95–100.

Virkamäki, A., K. Ueki, and C.R. Kahn. 1999. Protein-protein interaction in insulin signaling and the molecular mechanism of insulin resistance. *J. Clin. Invest.* 103:931–943.

Vogt, B., J.M. Carrascosa, B. Ermel, A. Ullrich, and H.U. Häring. 1991. The two isotypes of the human insulin receptor (HIR-A and HIR-B) follow different internalization kinetics. *Biochem. Biophys. Res. Commun.* 177:1013–1018.

Yamaguchi, Y., J.S. Flier, A. Yokota, H. Benecke, J.M. Backer, and D.E. Moller. 1991. Functional properties of two naturally occurring isoforms of the human insulin receptor in chinese hamster ovary cells. *Endocrinology.* 129: 2058–2066.

Yamamoto, M., Y. Toya, C. Schwencke, M.P. Lisanti, M.G. Myers, Jr., and Y. Ishikawa. 1998. Caveolin is an activator of insulin receptor signaling. *J. Biol. Chem.* 273:26962–26968.

Zacharias, D.A., J.D. Violin, A.C. Newton, and R.Y. Tsien. 2002. Partitioning of lipid-modified monomeric GFPs into membrane microdomains of live cells. *Science.* 296:913–916.

Zimmermann, T., J. Rietdorf, A. Girod, V. Georget, and R. Pepperkok. 2002. Spectral imaging and linear un-mixing enables improved FRET efficiency with a novel GFP2-YFP FRET pair. *FEBS Lett.* 531:245–249.